This article has been accepted for publication in a future issue of this journal, but has not been fully edited. Content may change prior to final publication. Citation information: DOI 10.1109/TPWRD.2014.2375556, IEEE Transactions on Power Delivery

Wideband Modeling, Field Measurement and Simulation of a 420 kV Variable Shunt Reactor

Bjørn Gustavsen, *Fellow, IEEE*, Magne Runde, and Trond M. Ohnstad

***Abstract*—A 420 kV gapped-core five-legged variable shunt reactor is modeled in the frequency range 5 Hz-10 MHz based on frequency sweep measurements and curve fitting. Comparison with time domain measurements at reduced voltage shows that the model can accurately predict the transient behavior of the shunt reactor, both for impinging overvoltages and circuit breaker transient recovery voltages. Among the observations is that mutual coupling between the phases leads to a beat phenomenon in the reactor voltage following disconnection. Representing the shunt reactor by an *LC* parallel circuit leads to unrealistic results for steep-fronted incoming waves and high-frequency oscillating overvoltages, and for the attenuation of the transient recovery voltage following disconnection.**

***Index Terms*—Variable shunt reactor, black-box model, frequency dependency, simulation, transients, transient recovery voltage, EMTP.**

I. Introduction

SHUNT reactors are used in the high-voltage grid as a means for controlling the voltage by compensating the reactive power production from overhead lines and underground cables. The switching in and out of shunt reactors by circuit breaker operation leads to transient phenomena which can disturb the system operation. For instance, energizing a cable having near 100% shunt compensation at its ends can lead to current zero-missing phenomena [1] which can temporarily prevent the circuit breaker from disconnecting the cable during a fault. Shunt reactor disconnection leads to a transient recovery voltage (TRV) across the circuit breaker contacts of a frequency of typically 1-5 kHz and a peak value which is strongly dependent on the circuit breaker chopping current [2], [3]. The transient models used in studying these phenomena are usually based on a parallel *LC* circuit ignoring any coupling between the phases [2], [3]. Although such simplified modeling is very practical and adequate for predicting the peak value of the TRV, it cannot be assumed to be valid over a very wide frequency range. Using a white-box model of a reactor, it has been shown [4] that the *LC* model may lead to incorrect estimates of the maximum overvoltages for fast transients.

In the case of power transformers, a number of works have been presented [5]-[10] where the transformer terminal behavior has been characterized over a wide frequency range using frequency sweep measurements with the transformer in short-circuit and/or hybrid conditions. From the sweep measurements, an EMTP-compatible simulation model can be extracted via curve fitting (e.g. vector fitting) and passivity enforcement, leading to a black-box model of the transformer. That approach is adopted in this work.

We describe the modeling of a 420 kV 90-200 MVA shunt reactor that is used in the Norwegian grid for voltage control. Since the reactor core is gapped, the terminal behavior can be expected to be reasonably linear; hence the black-box modeling approach using frequency sweep measurements is applied. The terminal admittance matrix is accordingly measured in the 5 Hz-10 MHz range using a dedicated measurement setup, and subjected to model extraction and passivity enforcement. The resulting model is validated by comparing measured and simulated frequency responses for the voltage transfer between the terminals with alternative loads, in both the frequency and the time domain. The accuracy is further validated by comparing measured and simulated transient recovery voltages when opening a switch. Using simulations alone, the model's voltage response to incoming steep fronted voltage waves is studied, and compared to what can be obtained by a simple *LC* circuit representation of the reactor.

II. Shunt Reactor Data

The unit is a 420 kV, three-phase 90-200 MVAR variable shunt reactor with solidly grounded neutral, operating at 50 Hz. The main electrical data for the transformer are given in Table I, for three alternative tap position settings, with *min*, *mid* and *max* referring to the number of connected turns. In this work, we considered the modeling for the reactor in position *mid* (130 MVAR).

TABLE I. Shunt Reactor Data

Tap position	*min*	*mid*	*max*
Q [MVAR]	200	130	90
L [H]	2.81	4.32	6.24

In addition, the manufacturer states a capacitance value of 16.66 nF, with bonded terminals and the neutral insulated from ground.

Manuscript received August 20, 2014.

Bjørn Gustavsen and Magne Runde are with SINTEF Energy Research, NO-7465 Trondheim, Norway (e-mail: bjorn.gustavsen@sintef.no). Trond Ohnstad is with Statnett, NO-0379 Oslo, Norway.

The work was supported by the Statnett. Additional support was provided by the Norwegian Research Council (RENERGI Programme), DONG Energy, EdF, EirGrid, Hafslund Nett, National Grid, Nexans Norway, RTE, Siemens Wind Power, and Statkraft.

0885-8977 (c) 2013 IEEE. Personal use is permitted, but republication/redistribution requires IEEE permission. See http://www.ieee.org/publications_standards/publications/rights/index.html for more information.

This article has been accepted for publication in a future issue of this journal, but has not been fully edited. Content may change prior to final publication. Citation information: DOI 10.1109/TPWRD.2014.2375556, IEEE Transactions on Power Delivery

The unit is a five-legged design where the three limbs associated with the windings are gapped. As a result, one can expect weak magnetic coupling between the windings, as well as a reasonably linear behavior of the core.

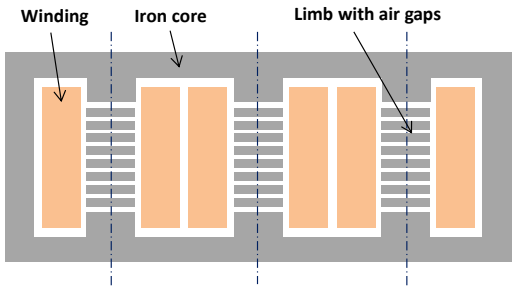

Fig. 1. Five legged core design.

III. Measurements

The measurements were performed in the field with the reactor terminals disconnected from the grid. Consequently, no other components (leads, busbars) could directly interfere with the measurements. Insulated wires (4-m) were connected to the transformer terminals and brought down to the base of the bushings where they were connected to shielded cables of 3-m length. The shielded cables were grounded locally at the bushing base and terminated in a connection box installed on the reactor top. The connection box has functionalities similar to the one described in [7], including a built-in wideband current sensor.

The connection box was used together with a Vector Network Analyzer (VNA) as described in [7] and shown in Fig. 3. Details about the current sensor and VNA are listed in Table II. This setup allows a direct measurement of the elements of the reactor terminal admittance matrix **Y** (3×3) which defines the relation (1) between terminal voltages **v** (3×1) and terminal currents **i** (3×1).

$$\mathbf{i}(\omega) = \mathbf{Y}(\omega)\,\mathbf{v}(\omega) \qquad (1)$$

Time domain responses were also measured on the connection box using the current sensor and 10 MΩ voltage probes.

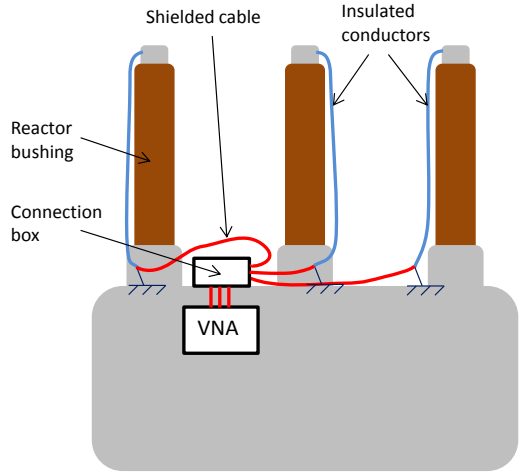

Fig. 2. Connecting measurement setup to the reactor terminals.

Fig. 3. Measurement of reactor admittance matrix.

TABLE II. List of Instruments

Current sensor	Ion Physics, model CM-100-6L
Vector network analyzer	Agilent ENA 5061B

IV. Modeling From Frequency Domain Responses

A. Initial Check on Measurement Accuracy

Using the VNA and connection box, diagonal element **Y**(2,2) was measured for tap positions *min*, *mid* and *max* in Table I, at 401 logarithmically spaced samples between 5 Hz and 10 MHz. Fig. 4 compares the measured element with the corresponding admittance $y=1/(j\omega L)$, where L is given in Table I. The measured low-frequency behavior is in good agreement with what can be inferred from manufacturer's data.

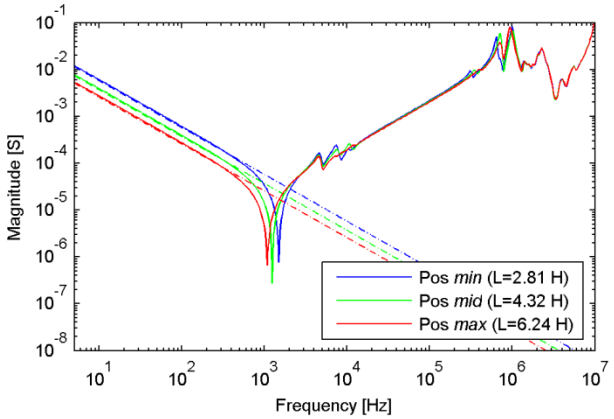

Fig. 4. Diagonal element $Y(2,2)$ at alternative tap positions (solid lines). Comparison with manufacturer's data $y=1/(j\omega L)$ (dashed lines).

B. Measurement and Model Extraction

The full admittance matrix **Y** was measured for tap position *mid* with the sampling density increased to using 1201 logarithmically spaced samples to better resolve the anti-resonance point in Fig. 4. The measured **Y** was subjected to pole-residue modeling (2) using Vector Fitting (VF) [11]-[13] with N=120 pole-residue terms. The extracted model is symmetrical and stable. Finally, the model was subjected to passivity enforcement by residue perturbation [14], [15] so as

0885-8977 (c) 2013 IEEE. Personal use is permitted, but republication/redistribution requires IEEE permission. See http://www.ieee.org/publications_standards/publications/rights/index.html for more information.

This article has been accepted for publication in a future issue of this journal, but has not been fully edited. Content may change prior to final publication. Citation information: DOI 10.1109/TPWRD.2014.2375556, IEEE Transactions on Power Delivery

to achieve a guaranteed stable simulation when included in a time domain simulation.

$$\mathbf{Y}(\omega) \cong \sum_{i=1}^{N} \frac{\mathbf{R}_i}{j\omega - a_i} + \mathbf{R}_0 + j\omega\mathbf{R}_{-1} \qquad (2)$$

Figs. 5 and 6 report the measured elements of **Y** and their approximation by the rational model (2). The agreement between measurement and model is seen to be very good. It is further observed that at low frequencies (50 Hz), **Y** is diagonal-dominant as is expected from the core design (five-legged with winding legs gapped). The magnitude of the largest off-diagonal element is only 2.6% of the smallest diagonal element. At frequencies around 1 MHz, there exists however a substantial coupling between the phases. Also, around the strong anti-resonance in the diagonal elements at about 1.2 kHz, the coupling is substantial as the off-diagonal elements are in magnitude almost equal to the diagonal elements.

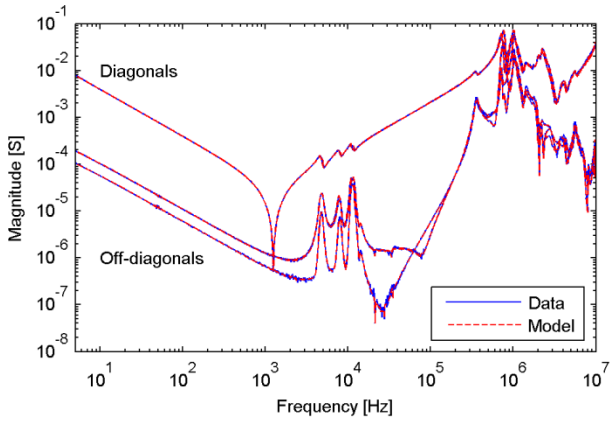

Fig. 5. Measured admittance matrix, **Y** (Tap pos. *mid*) and passive model extraction using N=120 poles. Magnitude functions.

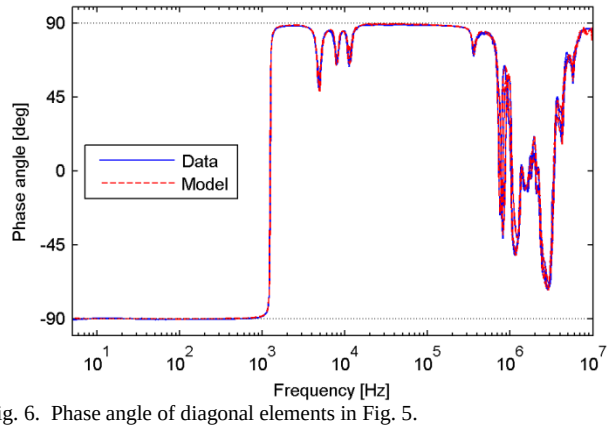

Fig. 6. Phase angle of diagonal elements in Fig. 5.

V. Frequency Domain Validation of Model in Voltage Transfer Calculations

In order to further validate the model, the voltage ratio from terminal 1 to terminals 2 and 3 was measured on the connection box using the VNA and voltage probes, and compared with those that can be inferred from the model. First, the loading effect of the voltage probes was accounted for by adding a shunt conductance of g=10^{-7} S to elements (2,2) and (3,3) of the calculated admittance **Y**(ω) of the model.

Next, the following partitioning (3) is introduced,

$$\mathbf{Y} = \begin{bmatrix} Y_{1,1} & Y_{1,2} & Y_{1,3} \\ Y_{2,1} & Y_{2,2} & Y_{2,3} \\ Y_{3,1} & Y_{3,2} & Y_{3,3} \end{bmatrix} = \left[\begin{array}{c|cc} Y_{1,1} & Y_{1,2} & Y_{1,3} \\ \hline Y_{2,1} & \multicolumn{2}{c}{\multirow{2}{*}{$\tilde{\mathbf{Y}}$}} \\ Y_{3,1} & & \end{array}\right] \qquad (3)$$

Combining (3) with (1) and using the condition i_1=0, i_2=0, the voltage ratios from terminal 1 to terminals 2 and 3 are obtained as

$$\begin{bmatrix} H_{2,1} \\ H_{3,1} \end{bmatrix} = \begin{bmatrix} V_2 / V_1 \\ V_3 / V_1 \end{bmatrix} = -\tilde{\mathbf{Y}}^{1-} \begin{bmatrix} Y_{2,1} \\ Y_{3,1} \end{bmatrix} \qquad (4)$$

Fig. 7 compares measured and calculated voltage ratios and shows an excellent agreement, except for below 1 kHz. Similar deviations at low frequencies resulted when basing the voltage ratio computation in (3) and (4) using the directly measured **Y**. The strong peak in the voltage transfer in Fig. 7 at 1.24 kHz corresponds to the anti-resonance in the diagonal elements of **Y** in Fig. 5 as a result of the matrix inversion in (4).

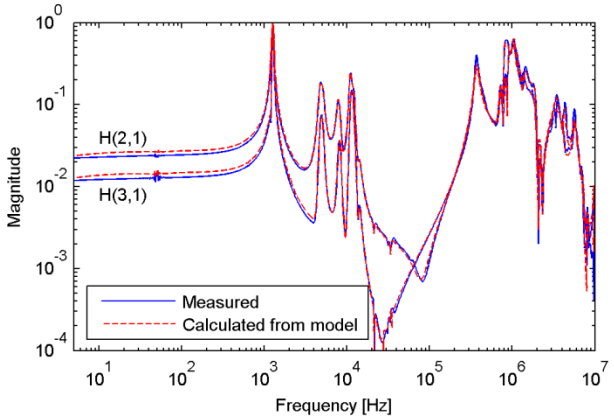

Fig. 7. Measured and calculated voltage ratios.

VI. Time Domain Validation of Model in Voltage Transfer Calculations

A. Voltage Transfer

In order to further validate the model, a step voltage was applied to terminal 1 and the voltage response on terminals 2 and 3 was measured, see Fig. 8. Using the applied voltage on terminal 1 as an ideal voltage source, the voltage on terminals 2 and 3 was simulated using the model. The effect of the voltage probes was accounted for by 10 MΩ resistors in the simulation.

Fig. 9 compares the measured and simulated voltage response on terminals 2 and 3, on a logarithmic time base. It is observed that a highly accurate result is obtained for the initial transient, while an offset results in the low-frequency oscillation which corresponds to the 1.24 kHz peak in the voltage transfer in Fig. 7. In an attempt to clarify the reason for this deviation, the voltage response was also calculated as the convolution between a rational model of the voltage transfer in Fig. 7 and the voltage excitation. This simulation resulted in about a 50% reduction of the low-frequency deviation.

Fig. 10 shows the same result after adding 401 Ω shunt

0885-8977 (c) 2013 IEEE. Personal use is permitted, but republication/redistribution requires IEEE permission. See http://www.ieee.org/publications_standards/publications/rights/index.html for more information.

This article has been accepted for publication in a future issue of this journal, but has not been fully edited. Content may change prior to final publication. Citation information: DOI 10.1109/TPWRD.2014.2375556, IEEE Transactions on Power Delivery

resistors to terminals 2 and 3, approximately representing the characteristic impedance of a connected overhead line. Comparison with Fig. 9 shows that the 1.23 kHz oscillation component has disappeared. This result is caused by the extremely high output impedance (>1 MΩ) at the reactor open terminals at 1.23 kHz, which is equal to the inverse of the corresponding admittance matrix diagonal elements.

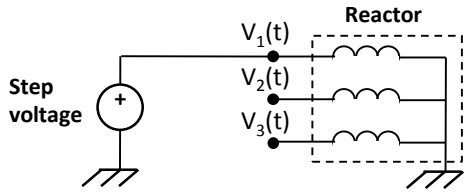

Fig. 8. Step voltage excitation.

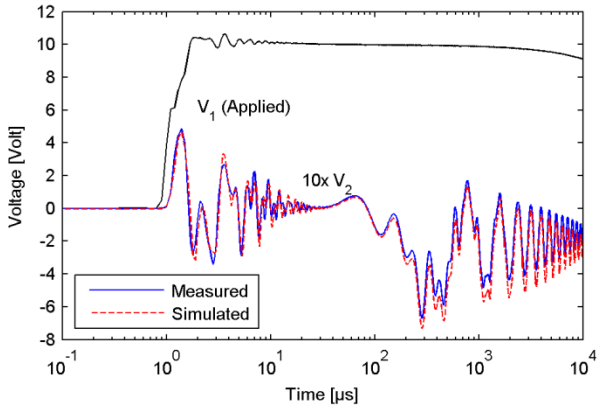

Fig. 9. Simulated and measured voltage on terminal 2 due to step voltage excitation on terminal 1.

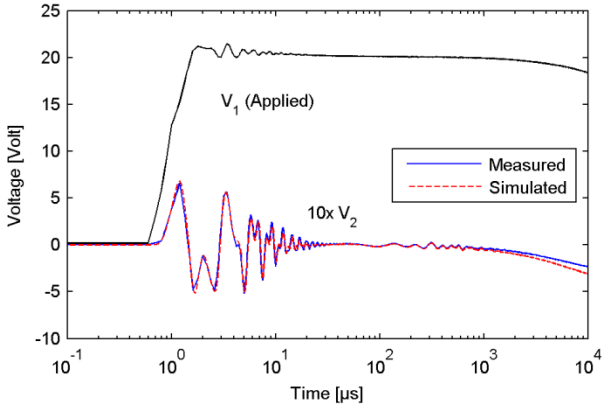

Fig. 10. Same result as Fig. 9, but with 401 Ω loads on open terminals.

VII. Time Domain Validation of Model in TRV Applications

A circuit breaker used for connecting the shunt reactor in the substation must be able to withstand the transient recovery voltage (TRV) that results when disconnecting the reactor. The TRV has a dominating frequency corresponding to the anti-resonance in admittance plots and a peak value which is twice that of the operating frequency. In practice, the current is chopped at a non-zero current value, and this increases the TRV peak value.

A. Measurements and Simulations

In order to simulate this scenario, a low-voltage sinusoidal source (function generator) with f=57.6 Hz was connected to one of the reactor terminals with the other terminals open, see Fig. 11. The source was removed by opening a mechanical switch. The voltage on the terminals was measured as well as the current through the switch.

The system was represented by an EMTP-like circuit simulator implemented in Matlab [16]. A time domain simulation was run where the measured voltage on the function generator output was used an ideal voltage source. The impact of the voltage probes was accounted for by introducing 10 MΩ shunt resistors in terminals 1, 2 and 3. The mechanical switch was in the simulation represented by an ideal switch that was open when the measured current is zero. The phasor representation of the voltage prior to opening the switch was calculated by fitting a sinusoidal model to the time domain waveform using non-linear optimization. The phasor solution was used to initialize the rational model to start the simulation without initial transients. The initialization procedure is similar to the one described in [17].

Fig. 12 shows the measured current together with the derived switch status, indicated with horizontal lines. It is observed that the breaker has one restrike. The measured pre-switching sinusoidal current has a peak value of 5.5 mA.

Figs. 13 and 14 show the voltage response on terminals 1 and 2, by measurement and by simulation. In the simulation, the switch status in Fig. 12 was used for controlling the opening and closing of the switch. It can be seen that a very accurate result has been obtained. The dominating frequency component is 1.23 kHz, corresponding to the anti-resonance in the admittance plot in Fig. 5. It can also be seen that a beat phenomenon results in the voltage on terminal 1 as energy is transferred to the oscillation in terminal 2 (and 3) and back.

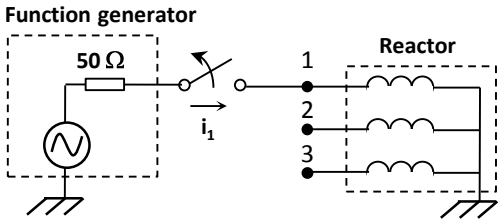

Fig. 11. Current interruption. Open @t=11.2 ms.

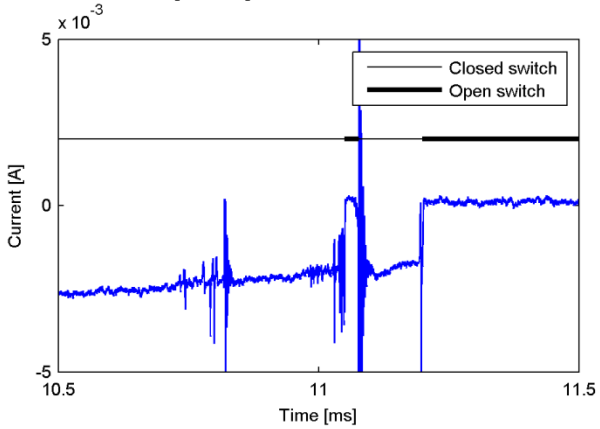

Fig. 12. Measured current response and switch status used in simulation.

0885-8977 (c) 2013 IEEE. Personal use is permitted, but republication/redistribution requires IEEE permission. See http://www.ieee.org/publications_standards/publications/rights/index.html for more information.

This article has been accepted for publication in a future issue of this journal, but has not been fully edited. Content may change prior to final publication. Citation information: DOI 10.1109/TPWRD.2014.2375556, IEEE Transactions on Power Delivery

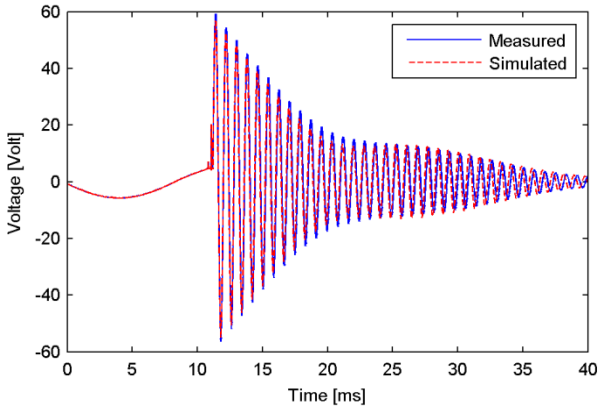

Fig. 13. Measured and simulated voltage response on terminal 1.

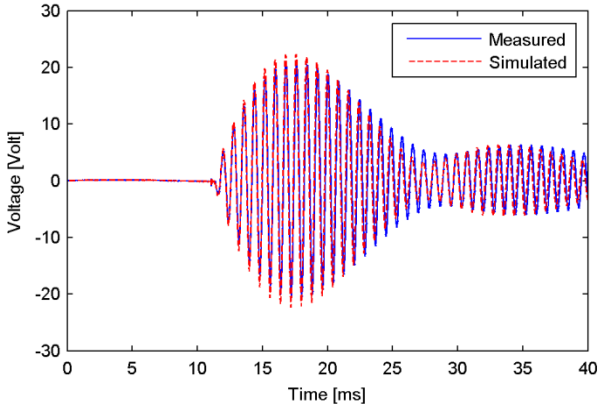

Fig. 14. Measured and simulated voltage response on terminal 2.

B. Voltage Transfer between Phases

The restrike observed in the current in Fig. 12 results in a temporary step voltage excitation on terminal 1, which induces a high-frequency transient voltage on terminals 2 and 3. Figs. 15 and 16 show the resulting current on terminal 2 at two different time scales, by measurement and simulation. It is seen that a good agreement is obtained for both the ~10 kHz oscillation (Fig. 15) and the ~1 MHz oscillation (Fig. 16).

C. Results Obtained Using LC Circuit Representation

IEEE [2] and IEC [3] recommend to model reactors by a parallel *LC* circuit in each phase, for the purpose of TRV calculations. A model was accordingly developed for the reactor in position *mid*. The resonance frequency of the parallel LC circuit is given as

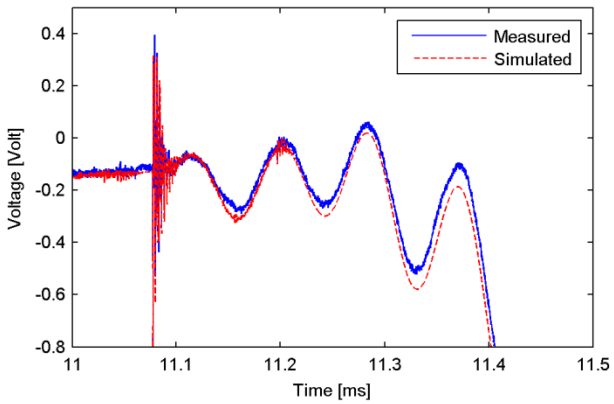

Fig. 15. Induced voltage on terminal 2 from restrike on terminal 1.

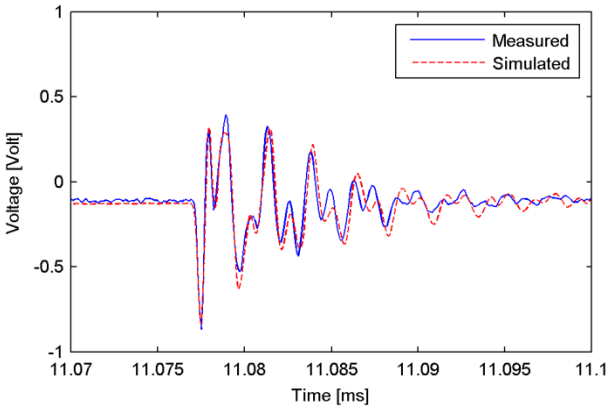

Fig. 16. Induced voltage on terminal 2. Zoomed view.

$$f = \frac{1}{2\pi\sqrt{LC}} \tag{5}$$

where f is the anti-resonance frequency in Fig. 5 (1.23 kHz). By solving (5) with L=4.32 H (Table I), we obtain a capacitance C=3.79 nF in phase 1. Fig. 17 compares the admittance of the LC model with that of the directly measured element $Y(1,1)$, showing a very good agreement up to about 400 kHz. The (small) coupling between phases is of course not represented by the *LC* model.

It has been proposed [18], [19] to improve the accuracy of the model by adding a resistor R in parallel with the LC circuit, obtained as

$$R = \frac{-\pi\sqrt{\frac{L}{C}}}{\ln(DF)} \tag{6}$$

where DF is a damping factor, being in the order of 0.6-0.8 for transformers [18].

Fig. 18 shows the simulation result by the *LC* model corresponding to the TRV example in Fig. 13, with DF=0.6, 0.8 and 1.0 (lossless). The results are compared with the measurements and the simulation result by the wide-band (WB)-model, for the initial transient. It can be seen that the proposed 0.6-0.8 range for DF is not appropriate for this reactor as the resulting damping is too high. It was found that a value of 0.9 gives a quite good agreement.

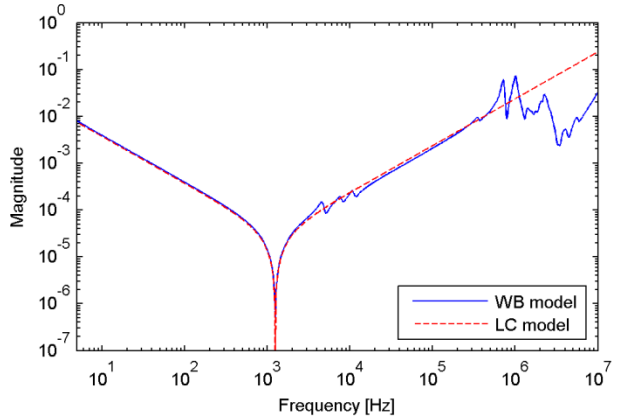

Fig. 17. Measured Element $Y(1,1)$ vs. LC response

0885-8977 (c) 2013 IEEE. Personal use is permitted, but republication/redistribution requires IEEE permission. See http://www.ieee.org/publications_standards/publications/rights/index.html for more information.

This article has been accepted for publication in a future issue of this journal, but has not been fully edited. Content may change prior to final publication. Citation information: DOI 10.1109/TPWRD.2014.2375556, IEEE Transactions on Power Delivery

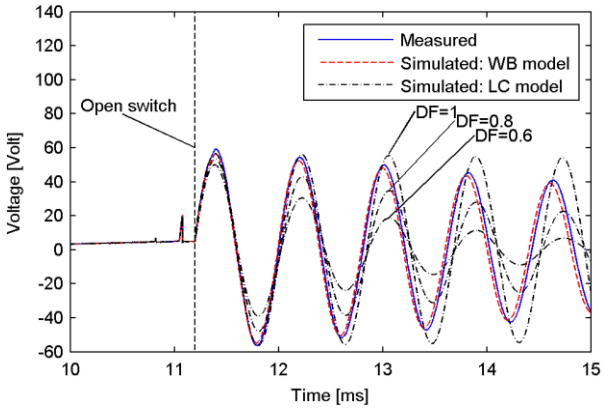

Fig. 18. Measured and simulated voltage response on terminal 1. Proposed wide-band (WB) model vs. *LC* parallel circuit with alternative damping factors.

VIII. Reactor Behavior With Steep-Fronted Waveforms

A. Transient Response to Incoming Waves

Shunt reactors are subjected to overvoltages resulting from switching operations in the substation, as well as faults and lightning strokes. When studying the resulting stresses on the reactor and neighboring equipment, a model must be used which accounts for the reactor's impact on the incoming waves. It is common practice to represent the reactor by an *LC* model, the capacitance alone, or simply ignoring the presence of the reactor.

Fig. 19 considers the case that a unit step voltage enters the reactor terminal 1 from a transmission line. The line is assumed lossless and of infinite length. Fig. 20 shows the voltage response on terminal 1 for three alternative values of the line characteristic impedance: 30 Ω (cable), 60 Ω (GIS), and 400 Ω (overhead line). The simulation result is shown when either representing the model using the wideband model developed in this work, or the lossless *LC* model. It can be seen that the *LC* model underestimates the front steepness of the initial voltage transient, as well as the oscillating component.

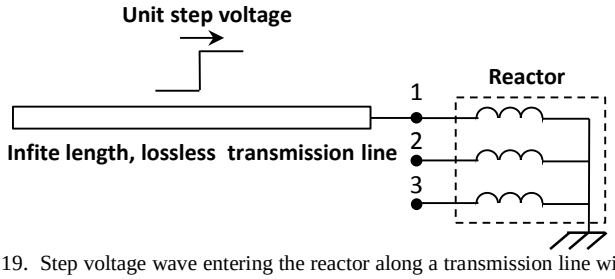

Fig. 19. Step voltage wave entering the reactor along a transmission line with alternative values for the line characteristic impedance.

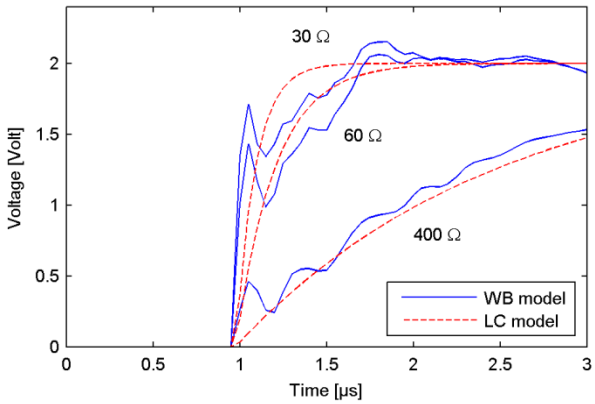

Fig. 20. Voltage response on reactor terminals due to incoming overvoltage on connected overhead line. Step voltage.

B. Damping of Resonant Overvoltages

The significance of including the oscillating components in the voltage response is in particular prevalent when studying high-frequency resonant overvoltages. Fig. 21 considers the situation that a short cable is energized from an infinite bus. The cable is an 800 mm^2 paper oil-type cable which is modeled by the Universal Line Model [20] as implemented in PSCAD. The propagation speed is 147 m/μs. By choosing the cable length as 43.8 m, the cable quarter wave resonance frequency becomes f=800 kHz which coincides with one of the anti-resonance frequencies observed in Fig. 17. The simulation result in Fig. 18 shows that the *LC* model gives a much too small damping of the oscillation. This inaccuracy is unacceptable if the simulation result is to be used as input for a study of internal overvoltages in the reactor by a white-box model [21].

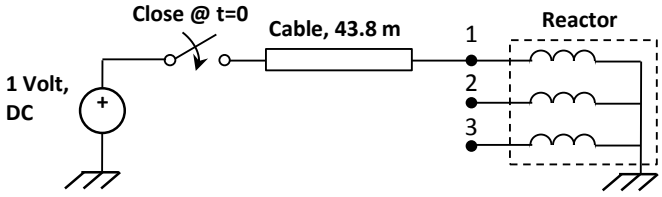

Fig. 21. Step voltage excitation on connecting cable.

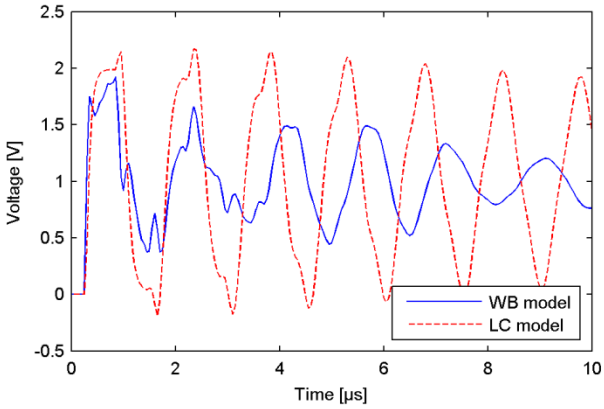

Fig. 22. Voltage response on reactor.

0885-8977 (c) 2013 IEEE. Personal use is permitted, but republication/redistribution requires IEEE permission. See http://www.ieee.org/publications_standards/publications/rights/index.html for more information.

This article has been accepted for publication in a future issue of this journal, but has not been fully edited. Content may change prior to final publication. Citation information: DOI 10.1109/TPWRD.2014.2375556, IEEE Transactions on Power Delivery

IX. Discussion

A. Circuit Breaker Chopping Current

The simulated results in Section VII may give the false impression that disconnecting a shunt reactor may produce overvoltages on the reactor in excess of 10 p.u. of the peak value of the normal phase-ground voltage. The reason for this exaggerated voltage is that the chopped current is unrealistically high compared to that occurring in a circuit breaker. In Fig. 11, the chopping current is 2.5 mA which is 45% of the peak value of the steady-state current (5.5 mA), before current interruption. For the given reactor in normal operation, the load current is 252 A, in tap position *mid*. With SF_6 breakers, the chopping current depends on several parameters including the breaker chopping number [3], but it rarely exceeds 10 A which amounts to only 3% of the peak value of the load current. Fig. 23 shows a simulation where the wideband reactor model is being disconnected from an infinite bus, assuming a chopping current of 10 A. The peak overvoltage on the reactor terminals now reaches only 2.2 p.u. We note that the beat in the overvoltages observed in Figs. 13 and 14 persist also in Fig. 23.

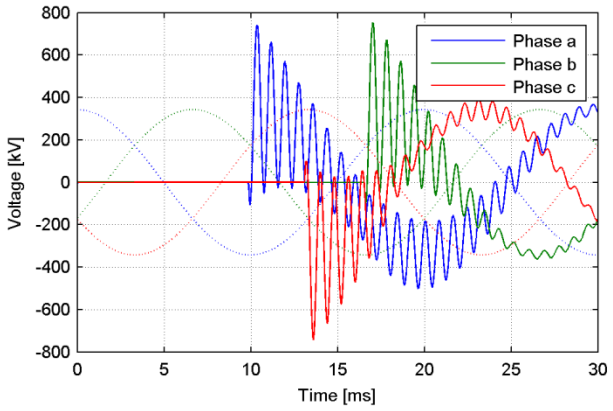

Fig. 23. Disconnecting shunt reactor operating at 420 kV, with 10 A chopping current.

B. Capacitance Value for LC circuit Modeling

When applying the *LC*-model it is necessary to find the proper capacitance value to use. From the measured admittance diagonal elements we estimated in Section VII-C a capacitance of 3.79 nF per phase, for tap position *mid*. From this value we must subtract 0.3 nF to account for the measurement cables, giving C=3.49 nF per phase. For comparison, the manufacturer stated a measured value of 16.66 nF with the three terminals and the neutral bonded, i.e. for the total shunt capacitance to ground. This amounts to 5.55 nF per phase. Of this, 0.63 nF (per phase) stems from the bushing. If the remaining shunt capacitance can be assumed to be equally distributed along the winding with the bottom part grounded, the effective capacitance seen from the terminals is according to a derivation in Greenwood's book [22] one-third of this capacitance, i.e. (5.55–0.63)/3=1.64 nF. In addition comes the 0.63 nF from the bushing, giving a total of 2.27 nF seen from the terminal. This value is much smaller than the 3.49 nF value found in this work. Among the possible reasons for this deviation are the contribution from the winding series capacitance and the interwinding capacitances, both being missing in the manufacturer's measurements. Reference [19] states that the effective capacitance for transformers is typically 0.4 times the measured (shunt) capacitance, but using this factor instead of Greenwood's 1/3 factor still gives a much too small value. We finally note that the capacitance as extracted from the admittance measurement (Fig. 4 and (5)) is dependent on the tap position as is shown in Table III.

TABLE III. Estimated Capacitance From Admittance Measurement

Tap position	*min*	*mid*	*max*
L [H]	2.81	4.32	6.24
f_0 [kHz]	1.50	1.23	1.08
C [nF]	3.48	3.79	4.02

It may be tempting to identify the capacitance via FRA measurements. Fig. 24 compares the measured element $Y(1,1)$ with correction for the measurement cable ($Y(1,1)(\omega)$–jωC, C=0.3 nF) with an end-to-end measurement on the transformer made by the manufacturer. Both results are with the reactor in the *max* position. It can be observed that the two curves differ very much as the current measurement is with FRA made at the reactor neutral side, thereby losing a significant part of the capacitive current. It is interesting to note that the first negative peak still coincides with the anti-resonance in the admittance measurement.

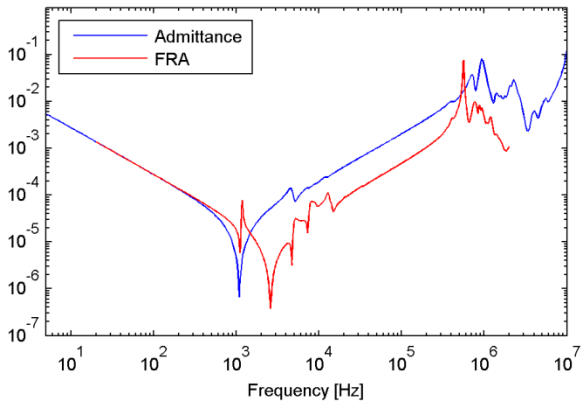

Fig. 24. FRA measurements vs. admittance measurement. Tap position *max*.

C. Reactor Model for Other Tap Settings

In this work we only created a model for the reactor in tap position *mid*. The procedure for frequency sweep measurements and model extraction is however general, and it can therefore be used for obtaining a wide-band model of the reactor in any tap position.

X. Conclusions

A wideband model has been developed for a 420 kV variable shunt reactor based on frequency sweep measurements at the reactor terminals followed by model extraction via curve fitting. The admittance matrix is measured between 5 Hz and 10 MHz using a dedicated setup, for the reactor in position *mid*. The following conclusions can be drawn from this work:

1. The voltage ratio between terminals as calculated by the admittance matrix agrees closely with measured voltage

0885-8977 (c) 2013 IEEE. Personal use is permitted, but republication/redistribution requires IEEE permission. See http://www.ieee.org/publications_standards/publications/rights/index.html for more information.

This article has been accepted for publication in a future issue of this journal, but has not been fully edited. Content may change prior to final publication. Citation information: DOI 10.1109/TPWRD.2014.2375556, IEEE Transactions on Power Delivery

ratios, demonstrating a high accuracy in the measurements, but with decreasing accuracy below 1 kHz.

2. A rational model is extracted from the admittance measurements using curve fitting and passivity enforcement, leading to a model that is compatible with EMTP-type circuit solvers.
3. The model is demonstrated to produce excellent results when compared to time domain simulation of voltage transfer between terminals, and in simulation of reactor TRV during reactor disconnection. The model is particularly well suited for calculating the voltage response to incoming steep-fronted voltages.
4. Usage of a simple *LC* model can also produce excellent results in TRV studies, but the determination of the capacitance is not always straightforward. Usage of admittance measurements appear to a safe way of obtaining the correct capacitance to be used.

XI. Acknowledgment

The authors appreciate the assistance of Oddgeir Rokseth during the measurements, as well as the substation staff, in particular Knut Dahl Hammervoll and Per Helge Langseth. Fredrik Vestbro at ABB Transformers, Ludvika, Sweden, is thanked for providing information regarding capacitance values and FRA measurements.

XII. References

[1] F.F. da Silva, C.L. Bak, and U.S. Gudmundsdottir, "Methods to minimize zero-missing phemomenon", *IEEE Trans. Power Delivery*, vol. 25. No. 4, pp. 2923-2930, Oct. 2010.

[2] D.F. Peelo and E.M. Ruoss, "A new IEEE Application guide for shunt reactor switching", *IEEE Trans. Power Delivery*, vol. 11, no. 2, pp. 881-887, April 1996.

[3] IEC 62271-110 Ed 3.0. High-voltage switchgear and controlgear - Part 110: Inductive load switching.

[4] S. Okabe, M. Koto, T. Teranishi, M. Ishikawa, T. Kobayashi, and T. Saida, "An electrical model of gas-insulated shunt reactor and analysis of re-ignition surge voltages", *IEEE Trans. Power Delivery*, vol. 14, no. 2, pp. 378-386, April 1999.

[5] A. Morched, L. Marti, and J. Ottevangers, "A high frequency transformer model for the EMTP," *IEEE Trans. Power Delivery*, vol. 8, no. 3, pp. 1615-1626, July 1993.

[6] M.J. Manyahi and R. Thottappillil, "Transfer of lightning transients through distribution transformers," *Proc. Int. Conf. Lightning Protection*, September 2-6, 2002, Cracow, pp. 435-440.

[7] B. Gustavsen, "Wide band modeling of power transformers", *IEEE Trans. Power Delivery*, vol. 19, no. 1, pp. 414-422, Jan. 2004.

[8] A. Borghetti, A. Morched, F. Napolitano, C.A. Nucci, and M. Paolone, "Lightning-induced overvoltages transferred through distribution power transformers", *IEEE Trans. Power Delivery*, vol. 24, no. 1, pp. 360-372, Jan 2009.

[9] B. Gustavsen, "A hybrid measurement approach for wide-band characterization and modeling of power transformers", *IEEE Trans. Power Delivery*, vol. 25, no. 3, pp. 1932-1939, July 2010.

[10] A. Holdyk, B. Gustavsen, I. Arana, J. Holboell, "Wide band modeling of power transformers using commercial sFRA equipment", *IEEE Trans. Power Delivery*, vol. 29, no. 3, pp. 1446-1453, June 2014.

[11] B. Gustavsen and A. Semlyen, "Rational approximation of frequency domain responses by vector fitting", *IEEE Trans. Power Delivery*, vol. 14, no. 3, pp. 1052-1061, July 1999.

[12] B. Gustavsen, "Improving the pole relocating properties of vector fitting", *IEEE Trans. Power Delivery*, vol. 21, no. 3, pp. 1587-1592, July 2006.

[13] D. Deschrijver, M. Mrozowski, T. Dhaene, and D. De Zutter, "Macromodeling of multiport systems using a fast implementation of the vector fitting method", *IEEE Microwave and Wireless Components Letters*, vol. 18, no. 6, pp. 383-385, June 2008.

[14] B. Gustavsen and A. Semlyen, "Enforcing passivity for admittance matrices approximated by rational functions", *IEEE Trans. Power Systems*, vol. 16, pp. 97-104, Feb. 2001.

[15] B. Gustavsen, "Fast passivity enforcement for pole-residue models by perturbation of residue matrix eigenvalues", *IEEE Trans. Power Delivery*, vol. 23, no. 4, pp. 2278-2285, October 2008.

[16] B. Gustavsen and H.M.J. De Silva, "Inclusion of rational models in an electromagnetic transients program – Y-parameters, Z-parameters, S-parameters, transfer functions", *IEEE Trans. Power Delivery*, vol. 28, no. 2, pp. 1164-1174, April 2013.

[17] B. Gustavsen and A. Portillo, "Interfacing k-factor based white-box transformer models with electromagnetic transients programs", *IEEE Trans. Power Delivery*, in press.

[18] IEEE special publication, *Modeling an analysis of system transients using digital programs*, IEEE Catalog Number 99TP133-0, 1998.

[19] R. Horton, R.C. Dugan, K. Wallace, and D. Hallmark, "Improved autotransformer model for transient recovery voltage (TRV) studies", *IEEE Trans. Power Delivery*, vol. 27, no. 2, pp. 895-901, April 2012.

[20] A. Morched, B. Gustavsen, and M. Tartibi, "A universal model for accurate calculation of electromagnetic transients on overhead lines and underground cables", *IEEE Trans. Power Delivery*, vol. 14, no. 3, pp. 1032-1038, July 1999.

[21] CIGRE Technical Brochure 577A, "Electrical transient interaction between transformers and the power system. Part 1 – Expertise", CIGRE JWG A2/C4.39, April 2014.

[22] A. Greenwood, *Electrical transients in power systems*, John Wiley & Sons, ISBN 978-0-471-62058-7.

XIII. Biographies

Bjørn Gustavsen (M'94–SM'2003–F'2014) was born in Norway in 1965. He received the M.Sc. degree and the Dr.Ing. degree in Electrical Engineering from the Norwegian Institute of Technology (NTH) in Trondheim, Norway, in 1989 and 1993, respectively. Since 1994 he has been working at SINTEF Energy Research where he is currently Chief Scientist. His interests include simulation of electromagnetic transients and modeling of frequency dependent effects. He spent 1996 as a Visiting Researcher at the University of Toronto, Canada, and the summer of 1998 at the Manitoba HVDC Research Centre, Winnipeg, Canada. He was a Marie Curie Fellow at the University of Stuttgart, Germany, August 2001–August 2002.

Magne Runde received the MSc degree in physics and the PhD degree in electrical power engineering from the Norwegian University of Science and Technology (NTNU), Trondheim, Norway, in 1984 and 1987, respectively. He has been with SINTEF Energy Research, Trondheim, Norway, since 1988. From 1996 to 2013 he was also an adjoint professor of high voltage technology at NTNU. His fields of interest include circuit breakers and switchgear, electrical contacts, power cables, diagnostic testing of power apparatus, and power applications of superconductors.

Trond M. Ohnstad was born in Oslo, Norway, on September 15, 1958. He graduated from the Faculty of Electrical Engineering, Oslo College, Oslo, Norway, in 1981. He has completed several special courses on power system planning, insulation coordination, surge protection, power electronics, and HVDC. His employment experience includes the Norwegian State Power Board, the Norwegian State Power Company, and the Norwegian Power Grid Company Statnett. His research interests are insulation coordination and surge protection, power quality, and power system transients.

0885-8977 (c) 2013 IEEE. Personal use is permitted, but republication/redistribution requires IEEE permission. See http://www.ieee.org/publications_standards/publications/rights/index.html for more information.